ACh-induced hyperpolarization and decreased resistance in mammalian type II vestibular hair cells.

LA Poppi[1], H Tabatabaee[1], HR Drury[1], P Jobling[1], RJ Callister[1], AA Migliaccio[2], PM Jordan[3], JC Holt[3], RD Rabbitt[4], R Lim[1] and AM Brichta[1]

Contributions

LA Poppi collected and analyzed experimental data (electrophysiology), and prepared figures/manuscript. **H Tabatabaee** collected experimental data (electrophysiology). **HR Drury** collected experimental data (electrophysiology). **P Jobling** advised on experimental technique (electrophysiology). **RJ Callister** advised on experimental technique (electrophysiology) and study aims. **AA Migliaccio** advised on data interpretation. **PM Jordan** and **JC Holt** collected and analyzed experimental data (immunofluorescence), and advised on data interpretation (immunofluorescence and electrophysiology). **RD Rabbitt** analysed and performed calculations on experimental data (capacitance measures), advised on data interpretation (electrophysiology) and assisted in developing the scope of the study. **R Lim** advised on experimental technique and data interpretation (all), assisted in developing the scope of the study, and edited the manuscript. **AM Brichta** (Principal Investigator) advised on experimental technique (all), developed the aims and scope of the study, advised on data interpretation (all) and edited the manuscript.

1. School of Biomedical Sciences and Pharmacy, The University of Newcastle and Hunter Medical Research Institute, Newcastle, NSW 2308, Australia.
2. Neuroscience Research Australia (NeuRA), Sydney, NSW 2031, Australia.
3. Department of Otolaryngology, University of Rochester, Rochester, NY 14642, USA.
4. Department of Bioengineering, University of Utah, UT 84112, USA.

Running Head

ACh responses in vestibular type II hair cells

Corresponding Author
Alan M. Brichta
Alan.Brichta@newcastle.edu.au
MS309 Medical Sciences Building
University Drive
The University of Newcastle
Callaghan
NSW 2308
Ph: +61 (2) 49217026

Number of pages: 36
Number of figures: 7, Number of tables: 1
Number of words: Abstract – 248, Introduction - 661, Discussion - 1972

ABSTRACT (248 words)

In the mammalian vestibular periphery, electrical activation of the efferent vestibular system (EVS) has two effects on afferent activity: 1) increases background afferent discharge; and 2) decreases afferent sensitivity to rotational stimuli. While the cellular mechanisms underlying these two contrasting afferent responses remain obscure, we postulated that the reduction in afferent sensitivity was attributed, in part, to the activation of alpha9-containing nAChRs (α9nAChRs) and small-conductance potassium channels (SK) in vestibular type II hair cells, as demonstrated in the peripheral vestibular system of other vertebrates. To test this hypothesis, we examined the effects of the predominant EVS neurotransmitter acetylcholine (ACh) on vestibular type II hair cells from wild type (wt) and α9nAChR-subunit knockout ($\alpha9^{-/-}$) mice. Immunostaining for choline acetyltransferase revealed there were no obvious gross morphological differences in the peripheral EVS innervation among any of these strains. ACh application onto wt type II hair cells, at resting potentials, produced a fast inward current followed by a slower outward current, resulting in membrane hyperpolarization and decreased membrane resistance. Hyperpolarization and decreased resistance were due to gating of SK channels. Consistent with activation of α9*nAChRs and SK channels, these ACh-sensitive currents were antagonized by the α9*nAChR blocker strychnine and SK blockers apamin and tamapin. Type II hair cells from $\alpha9^{-/-}$ mice, however, failed to respond to ACh at all. These results confirm the critical importance of α9nAChRs in efferent modulation of mammalian type II vestibular hair cells. Application of exogenous ACh reduces electrical impedance thereby decreasing type II hair cell sensitivity.

NEW & NOTEWORTHY (43 words)

Alpha 9 nicotinic subunit expression was crucial for fast cholinergic modulation of mammalian vestibular type II hair cells. These findings show a multifaceted efferent mechanism for altering hair cell membrane potential and decreasing membrane resistance that should reduce sensitivity to hair bundle displacements.

KEYWORDS

Vestibular efferent, calyx, alpha9, hair cell, nicotinic receptor, exocytosis.

INTRODUCTION

Vestibular efferent terminals appose type II hair cells, afferent bouton terminals, afferent fibers, and the outer surface of calyx terminals (Lysakowski and Goldberg 1997, 2004; Meredith and Roberts 1986; Purcell and Perachio 1997; Smith and Rasmussen 1968). There is compelling anatomical and physiological evidence in both mammalian and non-mammalian vertebrates that ACh is the primary neurotransmitter released by vestibular efferents (Guth et al. 1994; Holt et al. 2011; Housley and Ashmore 1991; Jordan et al. 2015). Vestibular efferent neurons express choline acetyltransferase (ChAT) (Jordan et al. 2015; Kong et al. 1998) and acetylcholinesterase (Carpenter et al. 1987; Gacek and Lyon 1974; Goldberg and Fernandez 1980; Hilding and Wersall 1962) while ACh receptor antagonists block responses evoked by efferent stimulation (Holt et al. 2006; Holt et al. 2015a; Rossi et al. 1980; Sugai et al. 1992). Conversely, when cholinergic agonists are applied to vestibular organs, the responses mimic those observed in efferent stimulation experiments (Guth et al. 1986; Holt et al. 2001; Holt et al. 2003).

Vestibular efferent stimulation has a profound impact on afferent nerve activity. In mammals, efferent stimulation increases background discharge rates of vestibular afferents (Goldberg and Fernandez 1980; Holt et al. 2015b; Marlinski et al. 2004; McCue and Guinan 1994), while reducing the sensitivity or gain of afferents to vestibular stimulation (Goldberg and Fernandez 1980). Although the precise mechanism(s) underlying the increased background discharge rate have not been positively identified, the reduction in sensitivity is putatively due to the activation of ACh receptors on vestibular type II hair cells (Holt et al. 2011; Kong et al. 2005; Kong et al. 2007; Rabbitt et al. 2009). Similar observations have been made in the cochlea (Doi and Ohmori 1993; Geisler 1974; Glowatzki and Fuchs 2000; Nenov et al. 1996) and in type II hair cells of the toadfish (Boyle et al. 2009).

Several nicotinic ACh receptor subunits, including alpha9 (α9), alpha10, alpha4, and beta2, are expressed by hair cells and afferents in the inner ear (Elgoyhen et al. 2001; Holt et al. 2003; Holt et al. 2015a; Luebke et al. 2005). Alpha9-containing nicotinic ACh receptors (α9*nAChRs) are critical for efferent inhibition of auditory hair cell and auditory afferent activity (Vetter et al. 1999). Based on data from auditory hair cells, the 'two-channel hypothesis' (Fuchs and Murrow 1992a, b) proposes ACh initiates a Ca^{2+} influx via α9*nAChRs that subsequently activates K^+ efflux and resistance reduction via small-conductance, Ca^{2+}-sensitive K^+ (SK) channels (Elgoyhen and Katz 2012; Oliver et al. 2000), and in some cases by opening BK channels (Rohmann et al. 2015). Opening of Ca^{2+}-sensitive K^+ channels lowers the membrane resistance and shunts the receptor current, thereby reducing sensitivity to hair bundle displacements (Geisler 1974; Rabbitt et al. 2009; Wiederhold and Peake 1966). In the mammalian vestibular system, it is unknown if α9*nAChRs and SK channels are also required for efferent control of hair cell sensitivity, but preliminary data suggest that mechanisms similar to auditory hair cells exist in mammalian type II vestibular hair cells (Kong et al. 2005; Poppi et al. 2014; Poppi et al. 2015; Yu et al. 2015).

Here we investigate cholinergic mechanisms at the efferent / vestibular type II hair cell synapse. In this study, α9 subunit knockout ($\alpha9^{-/-}$) mice were used to confirm the critical importance of α9 subunit expression for efferent function in type II hair cells. ChAT immunohistochemistry was used to examine peripheral EVS morphology while patch clamp methodologies and pharmacology were utilized to characterize the response of type II hair cells to ACh. Similar to auditory hair cells, mouse type II vestibular hair cells respond to ACh using a 'two-channel' mechanism. These results support the hypothesis that α9*nAChR-mediated reduction in type II hair cell membrane resistance contributes to the decreased sensitivity to motion stimuli observed in classical mammalian afferent recordings (Goldberg

and Fernandez 1980) following activation of the efferent vestibular system (EVS).

MATERIALS AND METHODS

Ethics Statement

All procedures described below were conducted in accordance with the University of Newcastle Animal Care and Ethics Committee guidelines. Immunofluorescence work at the University of Rochester was done using fixed tissue samples originating from the University of Newcastle.

Wildtype and knockout mice

In this study, we used two wildtype (wt) strains, CBA/CaJ x 129SvEvTac (CBA) and C57BL/6, to compare the effect of genetic background (*i.e.* CBA/CaJ;129 versus the readily available inbred strain, C57BL/6). The CBA strain was chosen because it is genetically similar, although not the same, as the background of the non-congenic homozygous alpha9 subunit knockout ($\alpha9^{-/-}$) strain provided by The Jackson Laboratory, USA (CBACaJ;129S-Chrna9tm1Bedv; RRID:IMSR_JAX:005696). The $\alpha9^{-/-}$ genotype was confirmed using standard PCR and the primer sequences recommended for this strain by the The Jackson Laboratory.

Immunofluorescent labeling of cholinergic terminals

Mice (all strains, either sex, aged 3-6 weeks) were anesthetized with ketamine (100 $mg.kg^{-1}$ i.p.). The anterior canals were clipped to allow fluid entry and the bony labyrinths were drop-fixed with fresh 4% paraformaldehyde for a minimum of 2 hrs at 4°C. Organs were placed in 0.1M phosphate-buffered saline (PBS) and rinsed several times over the course of 24 hours. For sections, cristae were dissected free, embedded in 4% agarose gel (Sigma), and sliced at 40 µm on a Leica CM1950 cryostat. Slices were then blocked with 10% normal goat serum (Sigma) and 0.5% Triton X-100 in 0.1M PBS for 1hr. Tissue was incubated overnight in primary antibodies against ChAT (1:200 in 0.1M PBS; Millipore Cat# AB144P Lot#

2280814 RRID: AB_11214092) and Myosin VIIa (1:200 in 0.1M PBS; Proteus Cat #25-6790, Lot#). Samples were washed with 0.1M PBS prior to the addition of anti-rabbit FITC (1:50 in PBS; Jackson IR Cat#711-095-152, Lot#120791) and anti-goat Texas Red (1:50 in PBS; Sigma Cat#SAB3700290 Lot#RI32452) and reacted for 2 hrs at room temperature. After washing with 0.1M PBS, samples were washed with distilled water, mounted onto Superfrost Plus Slides with *SlowFade*® Gold antifade mounting medium (ThermoFisher, Cat# P36930). Slides were subsequently imaged on a Nikon Eclipse C1 confocal laser-scanning microscope. Low power images were acquired using a 40X objective, Z-stack images were acquired with a 100X Plan-Apo oil immersion lens (z-slice thickness ~ 0.2 μm). Two-dimensional images were prepared using Image J software and three-dimensional renders were prepared in FluoRender (Wan et al. 2017).

ChAT immunohistochemistry and terminal morphology were also examined in crista whole organs. Similar to sections, whole crista were incubated overnight in antibodies against ChAT (1:100 in 0.1M PBS; Millipore Cat#AB144P Lot# JC1618187 RRID: AB_11214092), followed by 5 x 5 min washes with 0.1M PB prior to the addition of Alexa Fluor 488 donkey anti-goat secondary antibody (Invitrogen Cat#A-11055 RRID: AB_2534102) for 2 - 4 hours at room temperature. After another washing 5 x 5 mins with 0.1M PB, DAPI (1 μg/mL) was added for 5 minutes. Samples were washed with 0.1M PB and mounted onto slides as detailed above. Whole crista slides were imaged on a FV1000 confocal laser-scanning microscope, within the University of Rochester's Confocal Shared Resource. Z-stack images were acquired with a 100X Plan-Apo oil immersion lens (z-slice thickness 1 μm). Most whole organ image stacks were 70-100 μm in total depth. To prevent counting and measuring the same varicosities or terminals (puncta) within a single z-plane, every 10th z-section was used for puncta quantification. On average, seven z-plane images per organ were exported as TIFF files and then opened in the ImagePro Plus analysis program (RRID: SCR_007369)

where a manual threshold was set to select the varicosities and exclude the background. ChAT-positive puncta number and area were measured in ImagePro Plus using the count/measure feature within one to four, non-overlapping, 400 μm^2 areas of interest manually placed on the section image. In order to reduce extraneous noise, the lower size of the puncta area was set at 0.25 μm and following counting, the watershed algorithm was applied to help delineate between puncta that lay close to one another. Automated counts were comparable to blinded manual counts taken from same selected section. Data were exported into Microsoft Excel and GraphPad Prism (RRID: SCR_002798) for graphing and statistical analysis, respectively.

Patch-clamp recordings and ACh exposure

Mice (all strains, either sex, aged 3-6 weeks) were anesthetized with ketamine (100 $mg.kg^{-1}$ i.p.). Ketamine is a NMDA receptor antagonist that we, and others, have found to promote neuronal viability in *in vitro* preparations (de Oliveira et al. 2010). Once deeply anesthetized, mice were decapitated and the bony labyrinth isolated in ice-cold glycerol-modified Ringer's solution containing (in mM); 26 $NaHCO_3$, 11 glucose, 250 glycerol, 2.5 KCl, 1.2 NaH_2PO4, 1.2 $MgCl_2$ and 2.4 $CaCl_2$ and bubbled with Carbogen gas (pH 7.4; Ye et al. 2006). The vestibular triad – a semi-intact organ preparation comprising the anterior and horizontal crista, and utricle (Fig. 1A) – was excised, as described previously (Lim et al. 2011). The membranous roof overlying the neuroepithelium was removed, allowing access for whole-cell patch-clamp recordings. The triad was transferred to the recording chamber and continually perfused with oxygenated Leibovitz's L-15 cell culture medium (pH 7.55, Osm. 305 $mmol.kg^{-1}$; Life Technologies, Australia) at a rate of 4-6 bath exchanges / min. Whole-cell patch clamp recordings were obtained from type II vestibular hair cells in the anterior and horizontal cristae (Fig. 1B). Type II hair cells receive direct efferent input. Recording pipets were made from borosilicate glass (3 - 4 MΩ; King Precision Glass Inc., CA, USA)

filled with an internal solution containing (in mM) 42 KCl, 98 K.gluconate, 4 HEPES, 0.5 EGTA, 1 $MgCl_2$, 5 Na.ATP. In a subset of experiments, 10 mM BAPTA tetrapotassium salt (ThermoFisher Cat# B-1204) was substituted for EGTA in the internal solution. All experiments were done at room temperature (22°C). Type II hair cells were identified by their cylindrical profile, characteristic voltage-gated currents, the absence of a low-voltage activated potassium conductance ($G_{K,L}$).

ACh was applied within 10-20 µm of the recorded cell via a picospritzer driven pipet (Fig. 1B) at concentrations of 100 µM, 300 µM, and 1 mM; (Sigma; Cat# A6625). The picospritzer was programmed to deliver a bolus of ACh over 100 ms, to elicit reproducible ACh responses and minimize postsynaptic receptor desensitization. Intrinsic membrane properties, voltage activated currents, baseline holding current (or membrane potential) of type II hair cells were recorded before, during, and after ACh exposure. Recordings where series resistance (R_s) exceeded 20 MΩ or changed by >20% during the course of the recording session were excluded from analysis. Holding potentials varied from -96 mV to +4 mV to determine the voltage dependence of ACh-evoked currents. Antagonists (strychnine, apamin, - Sigma-Aldrich, Australia; iberiotoxin - Abcam, Australia; and tamapin - Alomone, Israel) were bath applied. Data was collected with Multiclamp 700B or Axopatch 1D amplifiers. Signals were sampled at 20 KHz, filtered at 10 KHz and digitized using Instrutech ITC16/USB16 A/D boards. Series resistance was compensated by 60% in all recordings, and voltages were corrected for liquid junction potentials (~6 mV for KCl-gluconate and ~8 mV for BAPTA-containing internals). Data was acquired and analyzed using AxoGraphX software (AxoGraphX, Sydney, Australia), and Igor Pro 6.3 (WaveMetrics Inc., OR, USA).

Membrane properties: Resistance (R_m) and Capacitance (C_m) measurements

We also measured series resistance (R_s), membrane resistance (R_m), and membrane capacitance (C_m). This was achieved using both time-domain and frequency-domain

methods. In the time-domain, we applied a standard 5 mV hyperpolarizing step pulse at the beginning, during, and at the completion of each cell recording to ensure recording conditions remained constant. In a subset of experiments, we continuously recorded R_m before, during, and after ACh exposure by superimposing one of two protocols onto the cell's holding potential. The time-domain protocol consisted of alternating ± 5 mV step pulses (3 ms duration, 2 ms separation). This protocol was used to monitor R_m every 10 ms. The frequency-domain protocol, consisted of a summation of three interrogation voltage sine waves (325, 525, 725 Hz) with a combined maximum peak-to-peak amplitude of 15 mV (± 7.5 mV) superimposed on top of the voltage command as described previously (Rabbitt et al., 2016). Similar to other methods (Farrell et al. 2006; Santos-Sacchi 2004), Fourier analysis of the current and voltage perturbations at the 3 interrogation frequencies was used to determine total access resistance R_s and whole-cell membrane impedance (effective capacitance C_m and resistance R_m) during the voltage command protocol. Briefly, the real and imaginary Fourier components of the current and voltage were extracted from the time domain data using a sliding Hanning window (over 15 periods, 40ms) for each of the 3 interrogation frequencies. Fourier components at the 3 interrogation frequencies were subtracted from the voltage command and whole cell current when displaying whole cell current. Data collected using a model cell with known electrical properties was used to determine the frequency-dependent transfer function necessary to calibrate the instrumentation for the specific voltage clamp protocols used. Separate transfer functions were calculated for the Axopatch and Multiclamp amplifiers and associated hardware. The method was verified by recording from alternative model cells and comparing the frequency domain Fourier analysis results to transient RC responses and known model cell parameters. Using three perturbation frequencies provides an over-determined set of equations (6 degrees of freedom) to estimate the three unknown parameters. Parameter estimation was done off-line using custom nonlinear least squares

software (Igor Pro 6.3).

RESULTS

Presence of cholinergic efferent terminals in wt and a9$^{-/-}$ mice

In this study, we used a semi-intact preparation of the anterior and horizontal cristae (Fig. 1A, B) that preserves much of the microstructure of the vestibular neuroepithelium (Lim et al. 2011). Cristae were collected from two wildtype strains (C57BL/6 and CBA) and α9$^{-/-}$ animals and processed for ChAT immunohistochemistry. In both wt (C57BL/6 and CBA) and α9$^{-/-}$ cristae, ChAT immunohistochemistry showed an extensive network of fibers and small en passant and terminal spherical varicosities (Fig. 1C - H), qualitatively similar to observations made in other mouse strains (Jordan et al. 2015; Luebke et al. 2014; Morley et al. 2017). Upon gross inspection, there were no obvious differences in varicosity morphology among these three strains of mice. Consistent with this assertion, the average number of ChAT-positive varicosities per 400 μm^2 in CBA cristae was not significantly different from counts performed in α9$^{-/-}$ mice cristae (16.1 ± 0.98 vs 14.5 ± 0.96, unpaired t test p = 0.35; n = 6). Our varicosity measurements, however, did suggest that mean ChAT-positive varicosity area in α9$^{-/-}$ cristae was significantly larger than mean varicosity area in CBA cristae (0.77 ± 0.05 vs 1.013 ± 0.06 μm^2; unpaired t test, p = 0.03; n = 6).

Characterizing cholinergic responses in type II vestibular hair cells

We used whole cell patch clamp recordings from both wt strains (CBA n = 62; C57BL/6 n = 41) and α9$^{-/-}$ (n = 88) mice to characterize ACh responses in type II vestibular hair cells. Type II vestibular hair cells were identified by their characteristic voltage-activated currents (Fig. 2A), and the absence of both the low-voltage activated potassium current, $I_{K,L}$, and a voltage-activated sodium current $I_{Nav,}$ that are prominent features of type I hair cells and calyx terminals, respectively (see review Eatock and Lysakowski 2006). R_m, C_m, and voltage-activated current properties in type II hair cells were similar in all three mouse strains (Table

1 and Fig. 2B). Recordings from type II hair cells in both wt strains (CBA and C57BL/6) were equivalent and therefore these data were pooled.

To determine the most appropriate concentration of ACh that would repeatedly evoke consistent responses over extended periods in type II hair cells, three initial concentrations of ACh (100 µM, 300 µM, and 1 mM) were applied by picospritzer onto wt type II hair cells. The lowest ACh concentration used, 100 µM, elicited responses that were smaller in amplitude relative to those evoked using higher ACh concentrations (n = 13, see Fig. 2C). The highest ACh concentration (1 mM) elicited currents that were similar in amplitude but longer in duration than responses evoked by 300 µM ACh (n = 7, Fig. 2C). Since there was no significant increase in amplitude during 1 mM exposures we concluded that 300 µM was sufficient to stimulate complete and reproducible ACh responses while minimizing the potential for receptor desensitization. The application of 300 µM ACh on a vestibular type II hair cell, at different holding potentials, is shown in Figure 2D. At -66 mV (Fig. 2D, black trace) the whole-cell current was biphasic, with a faster inward component followed by a slower outward component. The whole-cell current was fully inward at potentials more hyperpolarized than -70 mV, and predominantly outward at holding potentials of -50 mV and above. In current-clamp recordings, ACh hyperpolarizes type II hair cells (Fig. 2E). These observations are consistent with cholinergic signaling in other hair cell recordings whereby the early inward current represents α9nAChR activation whose calcium influx subsequently activates SK channels giving rise to the slow outward current.

The dependence of the outward current on calcium influx was revealed when 10 mM BAPTA was used in the internal solution instead of 0.5 mM EGTA. Here, the resulting ACh-induced inward currents were reduced by 90% and 41% at -68 mV and -48 mV, respectively. In addition, the outward currents were completely abolished by internal BAPTA at both potentials (n = 5 BAPTA, n = 5 EGTA; Fig. 2F, right panel). The absolute area under the

curve (charge) evoked by ACh was also reduced by 90% and 98% at -68 mV and -48mV, respectively. These altered responses are due to fast intracellular Ca^{2+} chelation by BAPTA. We conclude that Ca^{2+} entry through α9*nAChRs is critical to the normal ACh-induced currents shown in Fig. 2D, F (left panel), as well as the concomitant change in membrane impedance discussed below.

Cholinergic responses in type II hair cells require α9nAChRs

To confirm a role for α9*nAChRs, we characterized the response of vestibular type II hair cells to ACh under two conditions: (1) In wt mice before and during the application of the α9nAChR antagonist strychnine (Rothlin et al. 1999); and (2) in $\alpha9^{-/-}$ mice lacking the α9nAChR subunit. In wt mice, brief 100-ms pulses of 300 µM ACh on type II hair cells triggered extended current responses with at least two components that were dependent on membrane potential. At -46 mV, the response to ACh was composed of a small and brief inward current (Fig 3A, inset), followed by a much larger outward current (Fig 3A). At more negative potentials (-66mV and -96mV), the inward current dominated the response. In the presence of 1 µM strychnine, the ACh-evoked response was abolished at all holding potentials (Fig 3A; blue traces) suggesting ACh responses are dependent on α9*nAChRs. This was confirmed in $\alpha9^{-/-}$ mice where such ACh responses in type II hair cells were absent (Fig. 3B).

*Calcium influx through α9*nAChR activates SK channels in type II hair cells*

In the cochlea, activation of α9*nAChRs is coupled to two different types of Ca^{2+}-activated K^+ channels, termed BK and SK (Rohmann et al. 2015). To determine whether BK and/or SK channels might be involved in efferent signaling in vestibular organs, we examined the effects of blocking these two channels. The large outward current was insensitive to the BK channel antagonist, iberiotoxin (100 nM; n = 8, Fig. 4A left trace), but was very sensitive to

323 the SK channel antagonist, apamin (0.5 - 100 nM; n = 17, Fig. 4A middle trace, B) and
324 tamapin (50-100 nM; n = 3, Fig. 4A right trace), a preferentially SK2-selective antagonist. To
325 reveal the underlying SK component, we subtracted the average traces recorded in the
326 presence of apamin from control traces (Fig. 4C). These data suggest the reversal potential of
327 the SK-mediated current was between -70 and -75mV and confirms K^+ is the major charge
328 carrier for the apamin-sensitive current.

329 *Membrane resistance and capacitance measurements in wt and α9$^{-/-}$ type II hair cells*
330 To further explore the signaling capacity of ACh-mediated responses, we examined changes
331 in whole-cell resistance (ΔR_m) and capacitance (ΔC_m) using a multi-sine method. We first
332 confirmed that the multi-sine capacitance interrogation signal did not alter responses by
333 comparing ACh-evoked whole-cell currents to results obtained using standard voltage clamp.
334 Currents recorded using multi-sine protocol for wt (Fig 5A, thick black) and α9$^{-/-}$ (Fig. 5A,
335 red) at -66mV compare favorably to standard voltage clamp recordings (*e.g.* Fig. 4A-B at -
336 66 mV). When held at -66 mV, wt type II hair cells exhibited a significant ACh-induced
337 *decrease* in whole-cell resistance R_m (Fig. 5B). This reduction in R_m was similar to that
338 observed in toadfish type II hair cells during electrical stimulation of efferent fibers *in vivo*
339 (Boyle et al. 2009), suggesting similar responses might be present under physiological
340 conditions in mice. The average reduction in R_m for wt type II hair cells is illustrated in Fig.
341 5B (thick black trace) with maximum reduction after the stimulus of 511 MΩ (± 202, gray
342 band, n = 8). The total duration of ΔR_m matched the total duration of ΔI_m (vertical dotted gray
343 line). ΔI_m was biphasic, initially dominated by α9nAChRs and subsequently by SK channels,
344 while ΔR_m was strictly negative because both α9nAChRs and SK channels reduce the
345 membrane resistance when activated. There were negligible changes in I_m or R_m in α9$^{-/-}$ type
346 II hair cells during the same ACh exposure (Fig. 5A-B, respectively, thin red trace). Changes
347 were also near zero in wt type II hair cells when vehicle only (L-15) was applied via the same

picospritzer perfusion system (Fig, 5A-C, dashed blue trace). In summary, ACh-evoked a marked *decrease* in R_m in wt mammalian type II hair cells that was absent in $\alpha9^{-/-}$ type II hair cells.

In wt type II hair cells the ΔC_m response consisted of two components, 1) an initial ΔC_m transient increase (ΔC_m = 282 ± SD 157 fF, n = 8; Fig. 5C) with peak time and duration that paralleled the time course of ΔR_m; and 2) a smaller long-lasting increase (Fig 5D, ΔC_m =30.9 ± 13 fF, n = 8) that extended more than 60 seconds after ACh exposure. Alteration of capacitance due to mechanical membrane deformation associated with the application technique can be ruled out since there were no detectable C_m changes in response to application of vehicle alone (n = 3, blue dashed) or in $\alpha9^{-/-}$ hair cells. Both the transient and long-lasting increases in C_m were eliminated with BAPTA in the recording pipet (Fig. 5D, green dashed trace), demonstrating that intracellular calcium signaling was required for both components.

The observation that transient (<5s) and long-lasting (>60s) ΔC_m components were absent in $\alpha9^{-/-}$ hair cells (red solid traces), is consistent with results obtained using BAPTA in the pipet and further support the contention that calcium influx via efferent AChRs is required for ACh-evoked ΔC_m changes. The observations that: 1) transient ΔC_m time-dependent changes closely followed those of the SK conductance; 2) were eliminated by BAPTA; 3) and absent when α9 receptors had been knocked out, suggests the transient correlates with SK channel opening, but the specific origin of the displacement current was not investigated. Since the transient ΔC_m required intracellular $[Ca^{2+}]$ modulation and exhibited no significant voltage dependence (Fig. 5E), the displacement current was not a gating charge coupled to pore opening (Bezanilla 2000). As noted above, the long-lasting ΔC_m increases were present 60s after the stimulus, while the transient had a duration of <5s. Interestingly, we observed

similar, if not larger, ACh-evoked increases in ΔC_m at hyperpolarized holding potential of -91 mV (n = 3; Fig. 5E).

It should be noted, the lack of long-lasting ΔC_m in $\alpha9^{-/-}$ type II hair cells was not due to compromised capacitance changes associated with depolarization steps. These changes are thought to be the result of exocytosis since wt and $\alpha9^{-/-}$ type II hair cells both exhibited C_m increases in response to simple depolarizing voltage steps (Fig. 6). In an example from a wt type II hair cell, capacitance increases in response to 60 mV depolarizing pulses of 200 to 500 ms duration are shown in Fig. 6A. Cumulative increases in C_m for multiple depolarizations were the same for both wt and $\alpha9^{-/-}$ type II hair cells (Fig. 6B), suggesting exocytosis machinery was functional in all strains.

Effects of intracellular calcium chelation

As described above, intracellular BAPTA (10 mM) markedly reduced the ACh-evoked initial α9*nAChR inward current in type II hair cells by 77%, and completely abolished the secondary, SK channel outward current when measured in the time domain (n = 5; Fig. 2F). This pattern of altered ACh-evoked current response was replicated when using the frequency domain protocol ($\Delta I_{m;}$ Fig. 5A). In addition, the multi-sine protocol also revealed that BAPTA markedly reduced ΔR_m and blocked all ΔC_m responses to ACh application (Fig. 5B, C).

DISCUSSION

Recent behavioral work demonstrates that VOR adaptation and compensation are compromised in $\alpha9^{-/-}$ mice, suggesting the EVS and α9*nAChRs might be required for these important vestibular functions in mammals (Hubner et al. 2017; 2015). In primitive vertebrates, the EVS is known to play an important role in volitional movements and attention (Tricas and Highstein 1990), and similar functions involving α9*nAChRs might be relevant to mammals. Our study has examined the role of these receptors at the cellular level in mammalian vestibular type II hair cells, using $\alpha9^{-/-}$ animals and two strains of control mice.

Cholinergic varicosities and ChAT expression

The loss of ACh responsiveness in type II hair cells from the $\alpha9^{-/-}$ mice do not appear to be associated with any gross alterations in the peripheral EVS innervation patterns, at least with respect to canal cristae. We routinely observed vestibular efferent varicosities in the cristae of all three strains (Fig. 1). At face value, it was difficult to reconcile any obvious differences in ChAT-positive EVS neurons and varicosities in $\alpha9^{-/-}$ mouse crista as compared to the two control mouse strains examined in this study, or as compared to ChAT staining of EVS neurons in other mouse models, including a second independent $\alpha9^{-/-}$ strain where the morphological and ultrastructural organization of peripheral EVS varicosities appeared normal (Morley et al. 2017; Jordan et al. 2015; Luebke et al. 2014). In the mouse cochlea, loss of the α9nAChR subunit has been associated with changes in the number and size of efferent varicosities (Simmons and Morley 2011; Vetter et al. 1999; 2007). Although our quantitative analysis failed to identify any difference in the density of efferent varicosities between $\alpha9^{-/-}$ and CBA mice, it did reveal that efferent varicosities in $\alpha9^{-/-}$ animals may be larger. Background genetics inherent to maintaining the $\alpha9^{-/-}$ mutation on either a CBA/CaJ, a crossed CBA/CaJ × 129/SvEv, or a 129/SvEv line do not appear to contribute to the cochlear efferent phenotype observed in $\alpha9^{-/-}$mice (Vetter et al., 1999), suggesting that

differences in the size of cochlear efferent varicosities are a function of the loss of the α9nAChR subunit. However, given we have only characterized the EVS morphology and innervation patterns in CBA/CaJ x 129SvEvTac animals, we cannot eliminate the possibility that larger EVS varicosities in $\alpha9^{-/-}$ mice may be attributed to differences in background instead of, or in addition to, the loss of the α9nAChR subunit.

Hair cell recordings and ACh exposure

Our results show α9 subunit expression is necessary for normal cholinergic signaling at efferent/vestibular type II hair cell synapses in mice. We used 100-ms duration ACh applications, which triggered current and voltage responses that lasted several seconds (Fig. 2C, 2D). This is consistent with work in turtles and toadfish where responses in afferents and hair cells substantially outlasted the duration of efferent stimulation (Boyle et al. 2009; Brichta and Goldberg 2000).

It is known that α9*nAChRs are highly permeable and preferentially selective for Ca^{2+} (Doi and Ohmori 1993; Katz et al. 2000; Weisstaub et al. 2002) and intracellular Ca^{2+} concentration is elevated in vestibular hair cells following ACh exposure (Housley et al. 1990; Ohtani et al. 1994; Yamashita et al. 1993). The significant dampening effect of 10 mM internal BAPTA on whole-cell ACh responses (Fig. 2F) demonstrates the critical role of intracellular Ca^{2+} signaling in cholinergic modulation of vestibular hair cells.

The essential alpha9 nicotinic receptor subunit

The 'two channel hypothesis' describes the biphasic action of ACh on auditory hair cells (Fuchs and Murrow 1992a; Martin and Fuchs 1992) – a highly conserved mechanism across all vertebrates (Lustig 2006). ACh triggers Ca^{2+} influx via α9*nAChRs and a secondary Ca^{2+}-activated K^+ current that hyperpolarizes the hair cell (Glowatzki and Fuchs 2000; Housley and Ashmore 1991; Oliver et al. 2000) and decreases R_m (Boyle et al. 2009). We demonstrate

439 a similar mechanism also applies to mammalian vestibular type II hair cells. Between -66
440 and -46 mV, the ACh response comprises interplay between at least two components; an
441 initial, fast inward current and a secondary, slower outward current (Fig. 3A and inset). We
442 interpret the initial inward current as primarily Ca^{2+} through α9*nAChRs, and the outward
443 current as K^+ since at holding potentials more hyperpolarized than K^+ ion reversal (E_K = -85
444 mV), all ACh-induced current is inward (Fig. 3A). In wt mice, strychnine abolished ACh
445 responses suggesting that they are dependent on α9*nAChR activation (Fig. 3A), as shown in
446 frog and pigeon vestibular hair cells (Holt et al. 2001; Holt et al. 2003; Li and Correia 2011).
447 That $\alpha9^{-/-}$ mice lack these responses (Fig. 3B) confirm the critical importance of α9*nAChRs
448 for initiating the ACh response in vestibular type II hair cells.

449 *A role for calcium-sensitive K^+ channels*

450 In mouse vestibular cristae, the outward K^+ component of the ACh response was highly
451 sensitive to SK blockers, apamin and tamapin, whose picomolar concentrations favor SK2
452 (KCNN2, KCa2.2). In contrast, there were negligible effects of the BK blocker iberiotoxin
453 (Fig. 4A). Our observations are in contrast to those made in isolated guinea pig type II
454 vestibular hair cells, which showed sensitivity to iberiotoxin, but not to apamin (Kong et al.
455 2005). These contradictory results may be due to their enzymatic isolation of hair cells and/or
456 prolonged (seconds) ACh exposure. If BK was activated via calcium induced calcium release
457 (CICR), the prolonged ACh exposure and enzyme treatment might account for BK
458 recruitment over and above that we observed in our experiments. We used a semi-intact
459 preparation, without enzyme treatment (Lim et al. 2011) and only brief (100 ms), locally-
460 applied ACh to avoid receptor desensitization (Lee et al. 2015).
461 Although our ACh exposure was brief, the ensuing responses (ΔI_m, ΔR_m, and transient ΔC_m)
462 could last for several seconds, or several tens of seconds (long-lasting ΔC_m). These extended
463 effects may be the result of additional mechanisms at play. In addition to SK channels, initial

Ca^{2+} influx, via α9*nAChRs, may also trigger intracellular CICR (Castellano-Munoz et al. 2016; Sridhar et al. 1997) . Efferent-evoked CICR is thought to operate primarily through the closely associated 'synaptoplasmic cisterns' that store Ca^{2+} and amplify cholinergic responses, as described in cochlear hair cells (Evans et al. 2000; Kennedy and Meech 2002; Lioudyno et al. 2004). The close proximity of vestibular efferent synapses to an analogous structure may provide an additional pool of intracellular Ca^{2+} (Lysakowski and Goldberg 1997) to drive the SK response. While our current data support ACh-induced changes in intracellular Ca^{2+} concentration in vestibular hair cells, the potential involvement of Ca^{2+} stores was not addressed in this study.

In $\alpha9^{-/-}$ type II hair cells, the lack of functional α9*nAChRs means SK channel conductances could not be triggered by ACh exposure, eliminating the intracellular calcium signal required for activation of calcium activated K+ channels. Moreover, there was no compensatory up-regulation of other nAChR subtypes that triggered SK or BK channels in $\alpha9^{-/-}$ hair cells. Similarly, there were no detectable changes in voltage-activated currents (Fig. 4A, B) or passive membrane properties (*Table 1*) in $\alpha9^{-/-}$ hair cells compared to wt.

Membrane resistance (R_m) and acetylcholine

In previous toadfish, frog, and burbot studies, efferent stimulation decreased R_m of vestibular or lateral line hair cells by activation of basolateral conductances. Consistent with previous findings in toadfish (Boyle et al. 2009), present results in mouse demonstrate that the drop in R_m arises primarily from opening of [Ca^{2+}] activated K^+ channels and with voltage activated channels playing a much smaller role. EVS activation generates an electrical shunt in the basolateral membrane of the type II hair cell that reduces sensitivity by reducing voltage modulation in response to physiological mechano-electrical transduction (MET) currents (Boyle et al. 2009; Flock and Russell 1976; Sugai et al. 1992). This reduced sensitivity highlights a critical feature controlling the sensitivity of type II hair cells to ACh. Except for

studies in toadfish semicircular canals (Boyle et al. 2009) and outer hair cells (Geisler 1974; Rabbitt et al. 2009), this decreased gain response has perhaps been overshadowed by the excitatory action of ACh on vestibular afferent background discharge (Goldberg and Fernandez 1980; Holt et al. 2015a), and the emphasis on the hyperpolarizing effects in auditory hair cells (Glowatzki and Fuchs 2000; Goutman et al. 2005; Marcotti et al. 2004; Roux et al. 2011). The present report demonstrates that one source of the reduced afferent sensitivity after EVS activation in mammals in type II hair cells is likely due to α9*nAChR/SK-dependent reduction in hair cell resistance.

Membrane capacitance (C_m), acetylcholine, and calcium signaling

The importance of calcium signaling to ACh responses of type II hair cells was demonstrated by buffering intracellular calcium with BAPTA. Calcium buffering eliminated the ACh-evoked SK current and, like apamin (Fig. 4B), revealed the α9*nAChR current (green dotted, Fig. 5A). BAPTA also eliminated the transient capacitance increase, demonstrating a correlation between SK opening and ΔC_m (Fig. 5C). The present study did not examine causality or specific charges responsible for the transient change in capacitance. Intracellular BAPTA also eliminated the long-lasting (> 60s) capacitance increase (Fig. 5C-D). The long-lasting ACh-evoked capacitance increase implies an increase in membrane surface area, similar to the increase evoked by depolarizing voltage pulses (Fig. 6A). This raises the possibility of a link between efferent activation and hair cell neurotransmitter exocytosis. In immature cochlear inner hair cells, α9*nAChRs expression was needed for normal maturation of the ribbon synapse (Johnson et al. 2013). However, it is not known whether calcium influx through α9*nAChRs activation influences neurotransmitter exocytosis at the ribbon synapse. It has been shown previously in auditory hair cells that neurotransmitter vesicle release from ribbon synapses is related to available intracellular Ca^{2+} concentrations and CICR (Schnee et al. 2011). In the present experiments, long-lasting ACh-

induced capacitance increases were present under whole-cell voltage clamp conditions even at hyperpolarized holding potentials (e.g., -91 mV; Fig. 5E), minimizing the possibility of any calcium influx near the ribbon synapse through voltage activated Ca^{2+} channels. A consistent hypothesis is that ACh-evoked calcium entry through α9*nAChRs might have triggered neurotransmitter exocytosis leading to long-lasting capacitance increases.

It should also be noted that both the transient and long-lasting ΔC_m components are dependent on the presence of α9 subunit expression. Like the intracellular BAPTA results in wt mice, there was no net ΔC_m in $\alpha9^{-/-}$ type II hair cells under the same conditions (Fig. 5C). This lack of ACh-evoked ΔC_m in $\alpha9^{-/-}$ type II hair cells was not due to a transgenic alteration in the vesicular release mechanisms since depolarizing steps evoked ΔC_m increases in type II hair cells of all strains used, including $\alpha9^{-/-}$ (Fig. 6B). This supports the possibility of a Ca^{2+}-dependent link between α9*nAChRs and exocytosis in wt vestibular hair cells. If true, Ca^{2+}-dependent neurotransmitter release from type II hair cells could contribute to transient discharge rate increases in vestibular afferent neurons, particularly in calyx-bearing, functionally dimorphic afferents (Fig. 7A) during efferent activation (Goldberg and Fernandez 1980; Holt et al. 2015a; Rabbitt et al. 2010).

Intracellular Ca^{2+} and buffering

When considering intracellular Ca^{2+} there are two points to that need to be made. First, while the responses presented here are like those shown in other hair cell preparations, the exogenous application of 300 µM ACh may well evoke a response in the hair cell that differs from that which would occur following endogenous release of ACh from efferent terminals. It is plausible that 300µM ACh is driving a larger Ca^{2+} entry that overwhelms the cell's intrinsic intracellular Ca^{2+}-buffering capabilities, and therefore triggers neurotransmitter release where, under normal physiological conditions, it may not. The actual concentrations of ACh release at efferent terminals may be lower. Second, even though the methods and

internal solutions used are similar to other hair cell preparations, the intracellular Ca^{2+} buffering capacity is unknown and therefore may be altered by our whole-cell recording technique. Therefore, it remains to be determined if the mechanisms described, will occur under physiological conditions.

Decreased gain, increased activity.

Our data begin to reconcile three broadly accepted observations in response to vestibular efferent activation: 1) putative type II hair cell hyperpolarization in all mammalian species (Ashmore and Russell 1983; Holt et al. 2003; Housley et al. 1990; Kong et al. 2007); 2) decrease in irregular afferent sensitivity to physiological stimulation in mammals (Goldberg and Fernandez 1980); and 3) excitation in irregular afferent background discharge (Goldberg and Fernandez 1980).

Type II hair cells contact the majority of vestibular afferents, either as the exclusive hair cell inputs to bouton afferents, or as adjunct inputs to functional dimorphic afferent terminals (Fig. 7A). Therefore, any changes in type II hair cell activity will significantly influence peripheral output. Our results demonstrate that ACh released during efferent stimulation likely 'shunts' type II hair cells by opening α9*nAChRs and SK conductances thereby decreasing R_m . Together with outward K^+ current these responses would result not only in hair cell hyperpolarization but importantly, reduced voltage sensitivity to hair bundle MET currents driven by the reduction in R_m. In type II hair cells, Ca^{2+} influx through α9*nAChRs evoked long-lasting increases in C_m under whole-cell voltage-clamp, possibly due to an increase in membrane surface area triggered by calcium entry via AChRs (Fig. 7B), and subsequent activation of calcium-induced-calcium release CICR (Castellano-Munoz et al. 2016; Sridhar et al. 1997). Hence, efferent contact on type II vestibular hair cells could cause: 1) a *decrease* in sensitivity to physiological stimulation; and 2) a transient increase in

563 neurotransmitter exocytosis resulting in a transient *increase* in discharge rate of afferent

564 neurons that receive type II hair cell inputs.

	R_m (MΩ)	C_m (pF)	Peak I_K (nA)
C57BL/6 (n = 41)	518.6 ± 26.8	5.7 ± 0.4	3.0 ± 0.1
CBA/CaJ;129SvEVTac (n = 62)	593.4 ± 34.0	5.4 ± 0.3	3.1 ± 0.1
CBA129;A9$^{-/-}$ (n = 88)	599.5 ± 20.6	5.1 ± 0.3	3.0 ± 0.1

Table 1 – Comparison of intrinsic membrane properties in type II hair cells of C57BL/6, CBA and alpha9 knockout (α9$^{-/-}$) mice. Membrane resistance (R_m) and capacitance (C_m) were measured in all type II hair cell recordings with a ± 5 mV test pulse at a holding potential of -66 mV, using KCl-gluconate internal solution. Peak K^+ current (I_K) values were measured in all type II hair cells with a 80 mV depolarizing step from a holding potential of -66 mV. Values are represented as mean ± SEM. R_m, C_m, and Peak I_K values were not significantly different across the three mouse strains (p = 0.0583, p = 0.2224, and p = 0.3635 respectively: Kruskal-Wallis test). Since intrinsic membrane properties from wildtype strains (CBA and C57BL/6) were equivalent, these data were pooled and referred to as *wt*.

Figure 1. Semi-intact preparation of the mouse vestibular organs and cholinergic efferent varicosities. A. Semi-intact preparation of the mouse vestibular triad; anterior (AC) and horizontal cristae (HC), utricle (U) and vestibular nerve (VIII). Recording (R) and perfusion (P) pipets. Scale = 300 µm. **B.** Infra-red differential interference contrast optics image showing a recording pipet (R) in contact with type II hair cell, perfusion pipet (P) filled with 300 µM ACh dissolved in L-15, *eminentia* or *torus* of the anterior crista (*). Scale = 25 µm. **C, D, E.** Low power (40X) micrographs of canal cristae from all three strains immunostained with antibodies to choline acetyltransferase (ChAT, red) and Myosin VIIa (green). Scale bars represent 50 µm. **F, G, H.** Higher power (100X) z-projections of canal cristae from all three strains immunostained with antibodies to choline acetyltransferase (ChAT, red) and Myosin VIIa (green). Scale bars represent 10 µm. **I, J, K.** Higher power

(100X) 3D FluoRender images of hair cells and cholinergic terminals from all three strains. Scale bars represent 5 µm in planes *x*, *y*, *z*.

Figure 2. Type II hair cell recordings and responses to exogenous acetylcholine application. A. Activation profiles and **B.** I-V plot of wt and $\alpha9^{-/-}$ type II hair cells show no differences in voltage-activated currents. **C.** Example records of wt type II hair cell responses to 100 µM, 300 µM, and 1 mM ACh application at V_m = -66 mV using KCl-gluconate internal solution. **D.** Current responses to ACh (300 µM) at different holding potentials from -96 mV to -46 mV using KCl-gluconate internal solution. **E.** Current clamp recording in type II hair cell at resting membrane potential of -49 mV shows 300 µM ACh-evoked hyperpolarization. **F.** *Left*, Current responses to ACh (300 µM) application at V_m = -46 mV, -66 mV, and -96 mV using KCl-gluconate internal solution. *Right*, Attenuated responses at V_m = -48 mV, -68 mV, and -98 mV when using 10 mM BAPTA in the internal solution. *Note: Orange bar in all panels indicates onset and duration of ACh application (100 ms).*

Figure 3. Whole-cell acetylcholine responses in wt and $\alpha9^{-/-}$ type II hair cells. **A.** Example records showing a wt type II hair cell response to 300 µM ACh application (100 ms; orange bar) at different membrane holding potentials (V_m = -46 mV, -66 mV, and -96 mV; black traces). At -46 mV, ACh triggered a fast, small, inward current followed by a larger, slower, outward current (inset represents expansion of dashed rectangle). At -66 mV, a large inward current is followed by a relatively small outward current. At -96 mV only inward current is observed. All ACh induced currents were blocked with 1 µM strychnine (STR; blue traces). **B.** Example record showing an $\alpha9^{-/-}$ type II hair cell response to 300 µM ACh (100 ms; orange bar) at V_m = -46 mV, -66 mV, and -96 mV (red traces). Little or no responses were observed at the different holding potentials. All traces are the average of three consecutive repetitions.

Figure 4. Calcium-activated potassium conductance in type II hair cells following acetylcholine exposure. A. Example records showing three different wt type II hair cell responses to 300 µM ACh (100 ms; orange bars) at V_m = -46 mV. Outward current was insensitive to iberiotoxin (IBTX, 0.1 µM; left trace), but blocked by both apamin (APA, 0.1 µM; middle trace) and tamapin (TAM, 0.5 nM; right trace). **B.** Example record showing a wt type II hair cell response to 300 µM ACh (100 ms; orange bars) at V_m = -46 mV, -66 mV, and -96 mV (black traces). Apamin (APA, 0.1 µM) blocked calcium activated small potassium current (SK), revealing the primary α9nAChR (Ca^{2+}) current (green traces). **C.** At V_m = -46 mV, -66 mV, and -96 mV the APA record was subtracted from control traces to show the contribution of the SK current (grey traces). Each record is the average of three consecutive repetitions.

Figure 5. Acetylcholine evokes whole-cell changes in membrane current (ΔI_m), membrane resistance (ΔR_m) and membrane capacitance (ΔC_m). A. ACh (300 µM, 100 ms; orange bar) applied to type II hair cells, held at -66 mV. The average whole cell changes in membrane currents (ΔI_m) for wt (*wt ACh Avg*, n=8, thick dark gray trace), extracted from the multi-sine wave protocol, was the same as those collected with standard voltage protocol (see Fig. 2D at -66 mV). The dark gray trace shows the familiar ACh-evoked combination of inward and outward ionic currents. This response is in stark contrast to the average of $\alpha9^{-/-}$ responses (*$\alpha9^{-/-}$ ACh Avg*, n=5, red trace) where no detectable change in ΔI_m occurred. The shaded light grey (wt) and pink ($\alpha9^{-/-}$) areas reflect variability of responses across preparations, and this shading also applies to all subsequent panels. Thin black traces refer to a single example of wt response (*wt ACh*). Intracellular BAPTA (10 mM), a calcium chelator, significantly affected ΔI_m in response to ACh (wt ACh BAPTA; green dashed line). The inward current was diminished, while the outward current was abolished. This suggests that intracellular calcium is essential for normal ACh response in wt type II hair cells, but affects

SK activation more than α9nAChRs. No response is elicited when vehicle only (L-15; light blue dashed line) is used. **B.** Whole-cell R_m significantly decreased in wt ACh Avg during ACh application. The transient time course and duration (dashed vertical time line) of the change in wt R_m, paralleled the time course of wt ΔI_m (see, A). Note the wt ACh Avg current trace briefly passes through zero net current (ΔI_m, arrowhead), but still maintained a non-zero net change in membrane resistance (ΔR_m). Intracellular BAPTA reduced ΔR_m (green dashed line) and had a similar time course to ΔI_m in the presence of BAPTA. Also, there was no ΔR_m response in $\alpha 9^{-/-}$ cells or wt type II hair cells exposed to L15. **C.** ACh-evoked transient increases in ΔC_m in wt type II cells (black and dark grey traces), have the same time course as ΔI_m amd ΔR_m. No change in $\alpha 9^{-/-}$ type II hair cells (red trace) or wt cells exposed to vehicle only (L-15, light blue trace). **D.** Expanded time course of steady-state capacitance (60s after ACh application) shows a maintained average ΔC_m increase in wt cells (dark grey traces), but no change from baseline in $\alpha 9^{-/-}$ cells (red trace), vehicle only, or intracellular BAPTA. The average difference in ACh-evoked ΔC_m between wt and $\alpha 9^{-/-}$ cells was 30.9 ± 13 fF (mean ± SD). ΔC_m was significantly greater in wt than in $\alpha 9^{-/-}$ cells (wt= 22.1 ± 5.3 fF, n=8 versus $\alpha 9^{-/-}$ = -19.4 ± 18.2 fF, n=4; mean ± SD; Wilcoxon rank test, 2-tailed $p<0.05$). **E.** Transient ΔC_m increase in wt cells at V_m = -46 mV (grey trace), -66 mV (red trace), and -91 mV (green trace) in response to ACh (100ms, orange bar) and shows the transient capacitance changes are independent of holding potential and may even be larger under hyperpolarized conditions (-91 mV).

Figure 6. Depolarization evoked neurotransmitter release in type II hair cells of wt and $\alpha 9^{-/-}$ mice. A. Example record showing an increase in capacitance in a wt type II hair cell evoked by 60 mV, 200-500 ms depolarizing voltage steps from a holding potential of -66 mV. Asterisks indicate transient increases in capacitance, and square brackets indicate

658 'steady state' capacitance values between depolarizing steps. **B.** The cumulative increase in
659 'steady state' capacitance (fF) with depolarization step duration (s) was indistinguishable
660 between $\alpha9^{-/-}$ (red circles; n=3) and wt (grey triangles; n=5) strains, suggesting transmitter
661 release evoked by depolarization steps is normal in $\alpha9^{-/-}$ mice.

662 **Figure 7. A summary of anatomical contacts and ACh-evoked events associated with**
663 **mammalian type II hair cells**. **A**. Type II hair cells contact bouton afferents and functional
664 dimorphic afferents. In mammals, functional dimorphic afferents include conventional
665 dimorphic (1) arrangement, comprising calyx and bouton terminals (arrowheads), while
666 unconventional dimorphic (2) arrangement consist of calyx terminals with outer face (en
667 face) contacts (arrow) with type II hair cell (Lysakowski and Goldberg, 1997). Although the
668 prevalence of en face contacts has yet to be determined in mice, conventional dimorphic
669 units, comprise nearly 80% of some rodent species, and therefore could be directly affected
670 by proposed neurotransmitter exocytosis from type II hair cells. **B**. ACh released from
671 efferent terminals onto type II hair cells during efferent activation (orange terminal) triggers
672 influx of Ca^{2+} through α9 receptors (red), which results in the efflux of K^+ through SK
673 channels (blue). This ACh-evoked response has three effects: 1) a hyperpolarization of
674 membrane potential ($\downarrow V_m$); 2) a reduction in membrane resistance ($\downarrow R_m$); and 3) increased
675 membrane capacitance ($\uparrow C_m$). Hyperpolarization of V_m and reduced R_m would decrease type
676 II hair cell sensitivity to MET channel currents. Neurotransmitter exocytosis from type II hair
677 cells, indicated by long-lasting ΔC_m, could contribute to elevation of calyx-bearing afferent
678 background discharge by exciting their associated afferent bouton contacts and/or via direct
679 en face synaptic contact with calyx terminals.
680

REFERENCES

Ashmore JF, and Russell IJ. Sensory and effector functions of vertebrate hair cells. *J Submicrosc Cytol* 15: 163-166, 1983.

Bezanilla F. The voltage sensor in voltage-dependent ion channels. *Physiol Rev* 80: 555-592, 2000.

Boyle R, Rabbitt RD, and Highstein SM. Efferent control of hair cell and afferent responses in the semicircular canals. *J Neurophysiol* 102: 1513-1525, 2009.

Brichta AM, and Goldberg JM. Responses to efferent activation and excitatory response-intensity relations of turtle posterior-crista afferents. *J Neurophysiol* 83: 1224-1242, 2000.

Carpenter MB, Chang L, Pereira AB, Hersh LB, Bruce G, and Wu JY. Vestibular and cochlear efferent neurons in the monkey identified by immunocytochemical methods. *Brain Res* 408: 275-280, 1987.

Castellano-Munoz M, Schnee ME, and Ricci AJ. Calcium-induced calcium release supports recruitment of synaptic vesicles in auditory hair cells. *J Neurophysiol* 115: 226-239, 2016.

de Oliveira RB, Graham B, Howlett MC, Gravina FS, Oliveira MW, Imtiaz MS, Callister RJ, Lim R, Brichta AM, and van Helden DF. Ketamine anesthesia helps preserve neuronal viability. *J Neurosci Methods* 189: 230-232, 2010.

Doi T, and Ohmori H. Acetylcholine increases intracellular Ca2+ concentration and hyperpolarizes the guinea-pig outer hair cell. *Hear Res* 67: 179-188, 1993.

Eatock RA, and Lysakowski A. Mammalian Vestibular Hair Cells. In: *Vertebrate Hair Cells*, edited by Eatock RA, Fay RR, and Popper AN. New York: Springer-Verlag, 2006.

Elgoyhen AB, Vetter DE, Katz E, Rothlin CV, Heinemann SF, and Boulter J. alpha10: a determinant of nicotinic cholinergic receptor function in mammalian vestibular and cochlear mechanosensory hair cells. *Proc Natl Acad Sci U S A* 98: 3501-3506, 2001.

Elgoyhen AB, and Katz E. The efferent medial olivocochlear-hair cell synapse. *J Physiol Paris* 106: 47-56, 2012.

Evans MG, Lagostena L, Darbon P, and Mammano F. Cholinergic control of membrane conductance and intracellular free Ca2+ in outer hair cells of the guinea pig cochlea. *Cell Calcium* 28: 195-203, 2000.

Farrell B, Do Shope C, and Brownell WE. Voltage-dependent capacitance of human embryonic kidney cells. *Phys Rev E Stat Nonlin Soft Matter Phys* 73: 041930, 2006.

Flock A, and Russell I. Inhibition by efferent nerve fibres: action on hair cells and afferent synaptic transmission in the lateral line canal organ of the burbot Lota lota. *J Physiol* 257: 45-62, 1976.

Fuchs PA, and Murrow BW. A novel cholinergic receptor mediates inhibition of chick cochlear hair cells. *Proc Biol Sci* 248: 35-40, 1992a.

Fuchs PA, and Murrow BW. Cholinergic inhibition of short (outer) hair cells of the chick's cochlea. *J Neurosci* 12: 800-809, 1992b.

Gacek RR, and Lyon M. The localization of vestibular efferent neurons in the kitten with horseradish peroxidase. *Acta Otolaryngol* 77: 92-101, 1974.

Geisler CD. Model of crossed olivocochlear bundle effects. *J Acoust Soc Am* 56: 1910-1912, 1974.

Glowatzki E, and Fuchs PA. Cholinergic synaptic inhibition of inner hair cells in the neonatal mammalian cochlea. *Science* 288: 2366-2368, 2000.

Goldberg JM, and Fernandez C. Efferent vestibular system in the squirrel monkey: anatomical location and influence on afferent activity. *J Neurophysiol* 43: 986-1025, 1980.

Goutman JD, Fuchs PA, and Glowatzki E. Facilitating efferent inhibition of inner hair cells in the cochlea of the neonatal rat. *J Physiol* 566: 49-59, 2005.

730 **Guth PS, Norris CH, Guth SL, Quine DB, and Williams WH**. Cholinomimetics mimic
731 efferent effects on semicircular canal afferent activity in the frog. *Acta Otolaryngol* 102: 194-
732 203, 1986.
733 **Guth PS, Dunn A, Kronomer K, and Norris CH**. The cholinergic pharmacology of the
734 frog saccule. *Hear Res* 75: 225-232, 1994.
735 **Hilding D, and Wersall J**. Cholinesterase and its relation to the nerve endings in the inner
736 ear. *Acta Otolaryngol* 55: 205-217, 1962.
737 **Holt JC, Lioudyno M, Athas G, Garcia MM, Perin P, and Guth PS**. The effect of
738 proteolytic enzymes on the alpha9-nicotinic receptor-mediated response in isolated frog
739 vestibular hair cells. *Hear Res* 152: 25-42, 2001.
740 **Holt JC, Lioudyno M, and Guth PS**. A pharmacologically distinct nicotinic ACh receptor
741 is found in a subset of frog semicircular canal hair cells. *J Neurophysiol* 90: 1526-1536,
742 2003.
743 **Holt JC, Lysakowski A, and Goldberg JM**. Mechanisms of efferent-mediated responses in
744 the turtle posterior crista. *J Neurosci* 26: 13180-13193, 2006.
745 **Holt JC, Lysakowski A, and Goldberg JM**. The Efferent Vestibular System. In: *Auditory
746 and Vestibular Efferents*. New York: Springer-Verlag, 2011, p. 135-186.
747 **Holt JC, Kewin K, Jordan PM, Cameron P, Klapczynski M, McIntosh JM, Crooks PA,
748 Dwoskin LP, and Lysakowski A**. Pharmacologically distinct nicotinic acetylcholine
749 receptors drive efferent-mediated excitation in calyx-bearing vestibular afferents. *J Neurosci*
750 35: 3625-3643, 2015a.
751 **Holt JC, Jordan PM, and Schneider GT**. Pharmacological characterization of the synaptic
752 mechanisms governing the responses of mammalian vestibular afferents to efferent
753 stimulation. In: *Association for Research in Otolaryngology (ARO) Midwinter Meeting
754 Abstracts*. 38: 100, 2015b.

Housley GD, Norris CH, and Guth PS. Cholinergically-induced changes in outward currents in hair cells isolated from the semicircular canal of the frog. *Hear Res* 43: 121-133, 1990.

Housley GD, and Ashmore JF. Direct measurement of the action of acetylcholine on isolated outer hair cells of the guinea pig cochlea. *Proc Biol Sci* 244: 161-167, 1991.

Hubner PP, Khan SI, and Migliaccio AA. The mammalian efferent vestibular system plays a crucial role in vestibulo-ocular reflex compensation after unilateral labyrinthectomy. *J Neurophysiol* 117: 1553-1568, 2017.

Hübner PP, Khan SI, and Migliaccio AA. The mammalian efferent vestibular system plays a crucial role in the high-frequency response and short-term adaptation of the vestibuloocular reflex. *J Neurophysiol* 114: 3154-3165, 2015.

Johnson SL, Wedemeyer C, Vetter DE, Adachi R, Holley MC, Elgoyhen AB, and Marcotti W. Cholinergic efferent synaptic transmission regulates the maturation of auditory hair cell ribbon synapses. *Open Biol* 3: 130163, 2013.

Jordan PM, Fettis M, and Holt JC. Efferent innervation of turtle semicircular canal cristae: comparisons with bird and mouse. *J Comp Neurol* 523: 1258-1280, 2015.

Katz E, Verbitsky M, Rothlin CV, Vetter DE, Heinemann SF, and Elgoyhen AB. High calcium permeability and calcium block of the alpha9 nicotinic acetylcholine receptor. *Hear Res* 141: 117-128, 2000.

Kennedy HJ, and Meech RW. Fast Ca2+ signals at mouse inner hair cell synapse: a role for Ca2+-induced Ca2+ release. *J Physiol* 539: 15-23, 2002.

Kong WJ, Hussl B, Thumfart WF, and Schrott-Fischer A. Ultrastructural localization of ChAT-like immunoreactivity in the human vestibular periphery. *Hear Res* 119: 96-103, 1998.

Kong WJ, Guo CK, Zhang S, Hao J, Wang YJ, and Li ZW. The properties of ACh-induced BK currents in guinea pig type II vestibular hair cells. *Hear Res* 209: 1-9, 2005.

Kong WJ, Guo CK, Zhang XW, Chen X, Zhang S, Li GQ, Li ZW, and Van Cauwenberge P. The coupling of acetylcholine-induced BK channel and calcium channel in guinea pig saccular type II vestibular hair cells. *Brain Res* 1129: 110-115, 2007.

Lee AM, Wu DF, Dadgar J, Wang D, McMahon T, and Messing RO. PKCepsilon phosphorylates alpha4beta2 nicotinic ACh receptors and promotes recovery from desensitization. *Br J Pharmacol* 172: 4430-4441, 2015.

Li GQ, and Correia MJ. Responses of pigeon vestibular hair cells to cholinergic agonists and antagonists. *Brain Res* 1373: 25-38, 2011.

Lim R, Kindig AE, Donne SW, Callister RJ, and Brichta AM. Potassium accumulation between type I hair cells and calyx terminals in mouse crista. *Exp Brain Res* 210: 607-621, 2011.

Lioudyno M, Hiel H, Kong JH, Katz E, Waldman E, Parameshwaran-Iyer S, Glowatzki E, and Fuchs PA. A "synaptoplasmic cistern" mediates rapid inhibition of cochlear hair cells. *J Neurosci* 24: 11160-11164, 2004.

Luebke AE, Maroni PD, Guth SM, and Lysakowski A. Alpha-9 nicotinic acetylcholine receptor immunoreactivity in the rodent vestibular labyrinth. *J Comp Neurol* 492: 323-333, 2005.

Luebke AE, Holt JC, Jordan PM, Wong YS, Caldwell JS, and Cullen KE. Loss of alpha-calcitonin gene-related peptide (alphaCGRP) reduces the efficacy of the Vestibulo-ocular Reflex (VOR). *J Neurosci* 34: 10453-10458, 2014.

Lustig LR. Nicotinic acetylcholine receptor structure and function in the efferent auditory system. *Anat Rec A Discov Mol Cell Evol Biol* 288: 424-434, 2006.

Lysakowski A, and Goldberg JM. A regional ultrastructural analysis of the cellular and synaptic architecture in the chinchilla cristae ampullares. *J Comp Neurol* 389: 419-443, 1997.

Lysakowski A, and Goldberg JM. Morphophysiology of the Vestibular Periphery. In: *The Vestibular System*, edited by Highstein SM, Fay RR, and Popper AN. New York: Springer, 2004, p. 57-142.

Marcotti W, Johnson SL, and Kros CJ. Effects of intracellular stores and extracellular Ca(2+) on Ca(2+)-activated K(+) currents in mature mouse inner hair cells. *J Physiol* 557: 613-633, 2004.

Marlinski V, Plotnik M, and Goldberg JM. Efferent actions in the chinchilla vestibular labyrinth. *J Assoc Res Otolaryngol* 5: 126-143, 2004.

Martin AR, and Fuchs PA. The dependence of calcium-activated potassium currents on membrane potential. *Proc Biol Sci* 250: 71-76, 1992.

McCue MP, and Guinan JJ, Jr. Influence of efferent stimulation on acoustically responsive vestibular afferents in the cat. *J Neurosci* 14: 6071-6083, 1994.

Meredith GE, and Roberts BL. Central organization of the efferent supply to the labyrinthine and lateral line receptors of the dogfish. *Neuroscience* 17: 225-233, 1986.

Morley BJ, Lysakowski A, Vijayakumar S, Menapace D, and Jones TA. Nicotinic acetylcholine receptors regulate vestibular afferent gain and activation timing. *J Comp Neurol* 525: 1216-1233, 2017.

Nenov AP, Norris C, and Bobbin RP. Acetylcholine response in guinea pig outer hair cells. II. Activation of a small conductance Ca(2+)-activated K+ channel. *Hear Res* 101: 149-172, 1996.

Ohtani M, Devau G, Lehouelleur J, and Sans A. Cholinergic agonists increase intracellular calcium concentration in frog vestibular hair cells. *Hear Res* 80: 167-173, 1994.

Oliver D, Klocker N, Schuck J, Baukrowitz T, Ruppersberg JP, and Fakler B. Gating of Ca2+-activated K+ channels controls fast inhibitory synaptic transmission at auditory outer hair cells. *Neuron* 26: 595-601, 2000.

Poppi LA, Tabatabaee H, Callister RJ, Lim R, and Brichta AM. Cholinergic activity of the peripheral efferent vestibular system. *XXVII Bárány Society Meeting, Journal of Vestibular Research* 24, 2-3: 190, 2014.

Poppi LA, Tabatabaee H, Callister RJ, Jobling P, Migliaccio AA, Holt JC, Lim R, and Brichta AM. Fast cholinergic responses in cristae of control and alpha-9 knockout mice. In: *Association for Research in Otolaryngology (ARO) MidWinter Meeting Abstracts*. 38: 101, 2015.

Purcell IM, and Perachio AA. Three-dimensional analysis of vestibular efferent neurons innervating semicircular canals of the gerbil. *J Neurophysiol* 78: 3234-3248, 1997.

Rabbitt RD, Clifford S, Breneman KD, Farrell B, and Brownell WE. Power efficiency of outer hair cell somatic electromotility. *PLoS Comput Biol* 5: e1000444, 2009.

Rabbitt RD, Boyle R, and Highstein SM. Mechanical amplification by hair cells in the semicircular canals. *Proc Natl Acad Sci USA* 107: 3864-3869, 2010.

Rohmann KN, Wersinger E, Braude JP, Pyott SJ, and Fuchs PA. Activation of BK and SK channels by efferent synapses on outer hair cells in high-frequency regions of the rodent cochlea. *J Neurosci* 35: 1821-1830, 2015.

Rossi ML, Prigioni I, Valli P, and Casella C. Activation of the efferent system in the isolated frog labyrinth: effects on the afferent EPSPs and spike discharge recorded from single fibres of the posterior nerve. *Brain Res* 185: 125-137, 1980.

Rothlin CV, Katz E, Verbitsky M, and Elgoyhen AB. The alpha9 nicotinic acetylcholine receptor shares pharmacological properties with type A gamma-aminobutyric acid, glycine, and type 3 serotonin receptors. *Mol Pharmacol* 55: 248-254, 1999.

Roux I, Wersinger E, McIntosh JM, Fuchs PA, and Glowatzki E. Onset of cholinergic efferent synaptic function in sensory hair cells of the rat cochlea. *J Neurosci* 31: 15092-15101, 2011.

Santos-Sacchi J. Determination of cell capacitance using the exact empirical solution of partial differential Y/partial differential Cm and its phase angle. *Biophys J* 87: 714-727, 2004.

Schnee ME, Santos-Sacchi J, Castellano-Munoz M, Kong JH, and Ricci AJ. Calcium-dependent synaptic vesicle trafficking underlies indefatigable release at the hair cell afferent fiber synapse. *Neuron* 70: 326-338, 2011.

Simmons DD, and Morley BJ. Spatial and temporal expression patterns of nicotinic acetylcholine alpha9 and alpha10 subunits in the embryonic and early postnatal inner ear. *Neuroscience* 194: 326-336, 2011.

Smith CA, and Rasmussen GL. Nerve endings in the maculae and cristae of the chinchilla vestibule, with a special reference to the efferents. *Third symposium on the role of the vestibular organs in space exploration* 152: 183-201, 1968.

Sridhar TS, Brown MC, and Sewell WF. Unique postsynaptic signaling at the hair cell efferent synapse permits calcium to evoke changes on two time scales. *J Neurosci* 17: 428-437, 1997.

Sugai T, Yano J, Sugitani M, and Ooyama H. Actions of cholinergic agonists and antagonists on the efferent synapse in the frog sacculus. *Hear Res* 61: 56-64, 1992.

Tricas TC, and Highstein SM. Visually mediated inhibition of lateral line primary afferent activity by the octavolateralis efferent system during predation in the free-swimming toadfish, Opsanus tau. *Exp Brain Res* 83: 233-236, 1990.

Vetter DE, Liberman MC, Mann J, Barhanin J, Boulter J, Brown MC, Saffiote-Kolman J, Heinemann SF, and Elgoyhen AB. Role of alpha9 nicotinic ACh receptor subunits in the development and function of cochlear efferent innervation. *Neuron* 23: 93-103, 1999.

Vetter DE, Katz E, Maison SF, Taranda J, Turcan S, Ballestero J, Liberman MC, Elgoyhen AB, and Boulter J. The alpha10 nicotinic acetylcholine receptor subunit is

878 required for normal synaptic function and integrity of the olivocochlear system. *Proc Natl*
879 *Acad Sci U S A* 104: 20594-20599, 2007.
880 **Wan Y, Otsuna H, Holman HA, Bagley B, Ito M, Lewis AK, Colasanto M, Kardon G,**
881 **Ito K, and Hansen C**. FluoRender: joint freehand segmentation and visualization for many-
882 channel fluorescence data analysis. *BMC Bioinformatics* 18: 280, 2017.
883 **Weisstaub N, Vetter DE, Elgoyhen AB, and Katz E**. The alpha9alpha10 nicotinic
884 acetylcholine receptor is permeable to and is modulated by divalent cations. *Hear Res* 167:
885 122-135, 2002.
886 **Wiederhold ML, and Peake WT**. Efferent inhibition of auditory-nerve responses:
887 dependence on acoustic-stimulus parameters. *J Acoust Soc Am* 40: 1427-1430, 1966.
888 **Yamashita T, Ohnishi S, Ohtani M, and Kumazawa T**. Effects of efferent
889 neurotransmitters on intracellular Ca2+ concentration in vestibular hair cells of the guinea
890 pig. *Acta Otolaryngol Suppl* 500: 26-30, 1993.
891 **Ye JH, Zhang J, Xiao C, and Kong JQ**. Patch-clamp studies in the CNS illustrate a simple
892 new method for obtaining viable neurons in rat brain slices: glycerol replacement of NaCl
893 protects CNS neurons. *J Neurosci Methods* 158: 251-259, 2006.
894 **Yu Z, Sadeghi S, McIntosh JM, and Glowatzki E**. Mechanisms of cholinergic efferent
895 synaptic inputs to vestibular type II hair cells. In: *Association for Research in Otolaryngology*
896 *(ARO) MidWinter Meeting Abstracts*. 38: 389, 2015.
897
898

ACKNOWLEDGEMENTS

This study was funded by the National Health and Medical Research Council (NHMRC) of Australia (Grant number: 1011159) and the Garnett Passe & Rodney Williams Memorial Foundation (Australia).

CONFLICT OF INTEREST

The authors declare no competing financial interests.

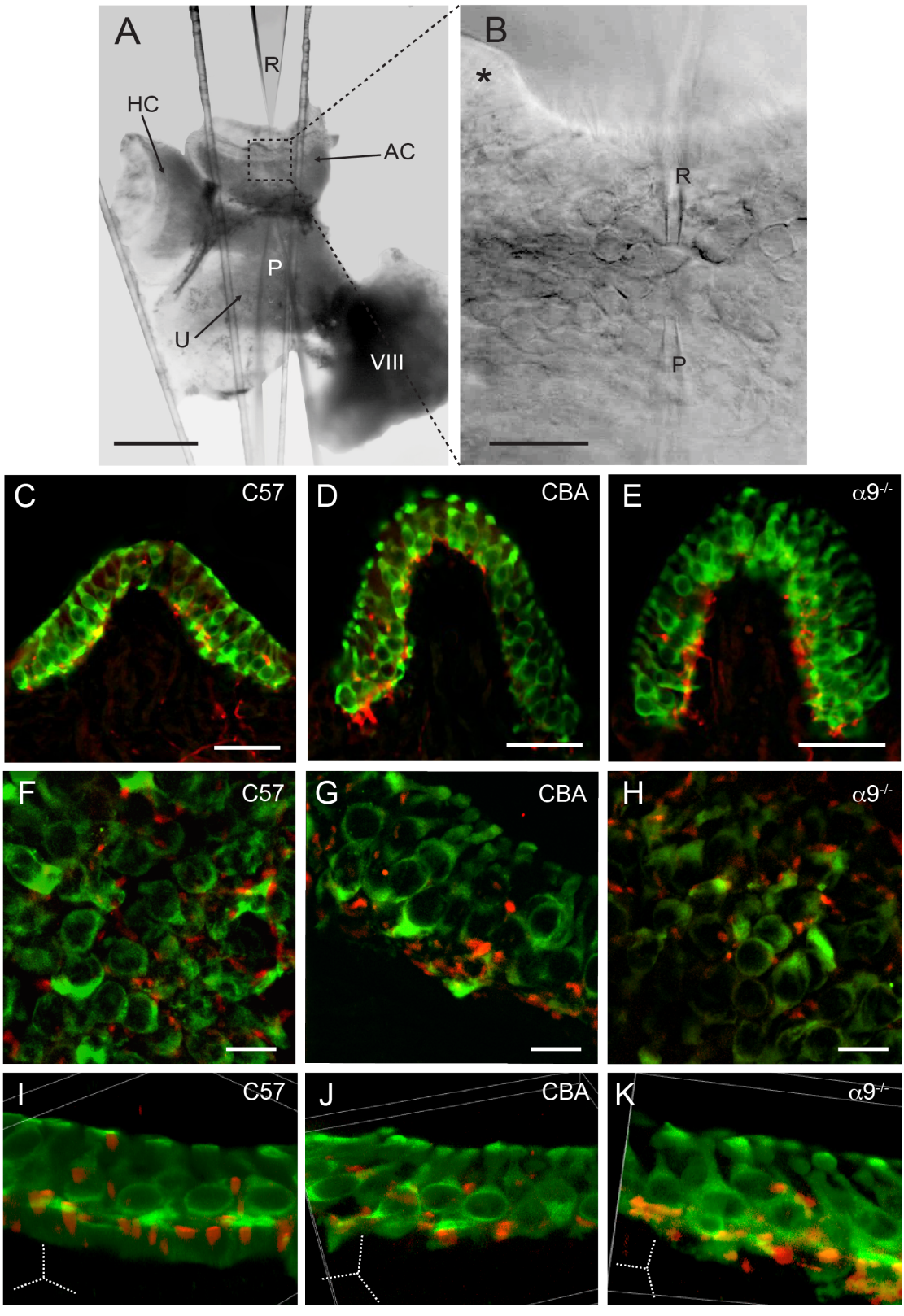

Figure 1 - Poppi *et al.* (2017) - R2

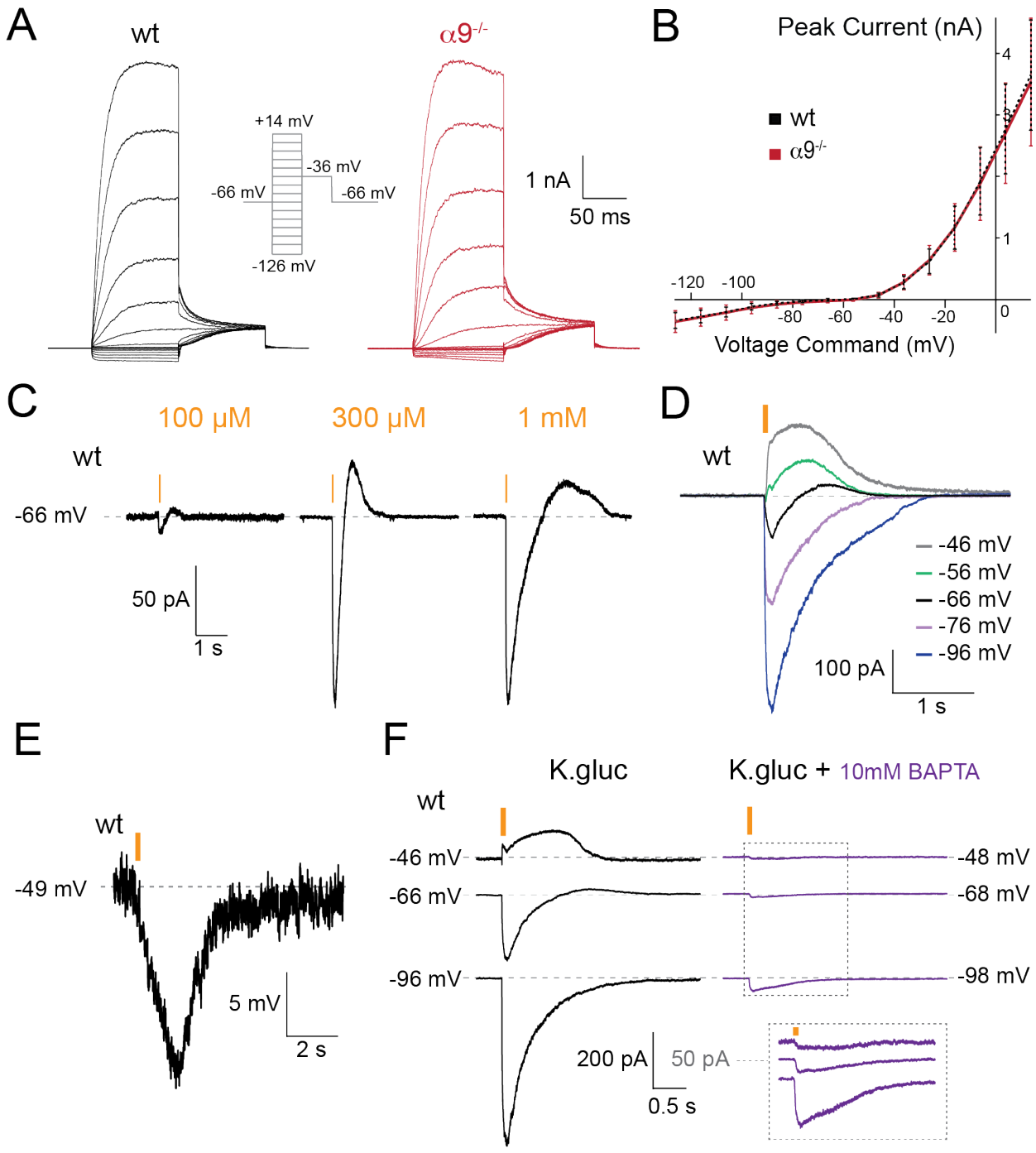

Figure 2 Poppi et al. (2017) - R2

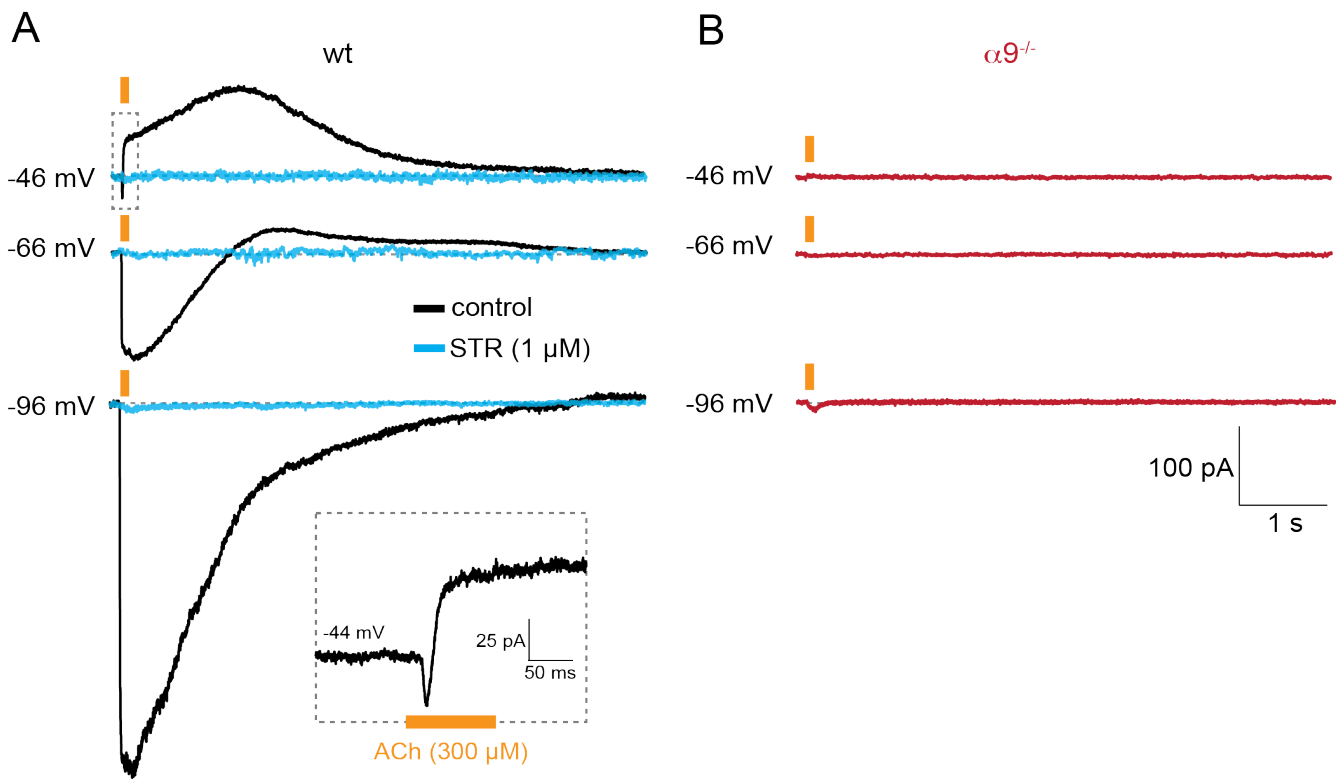

Figure 3 Poppi et al. (2017)

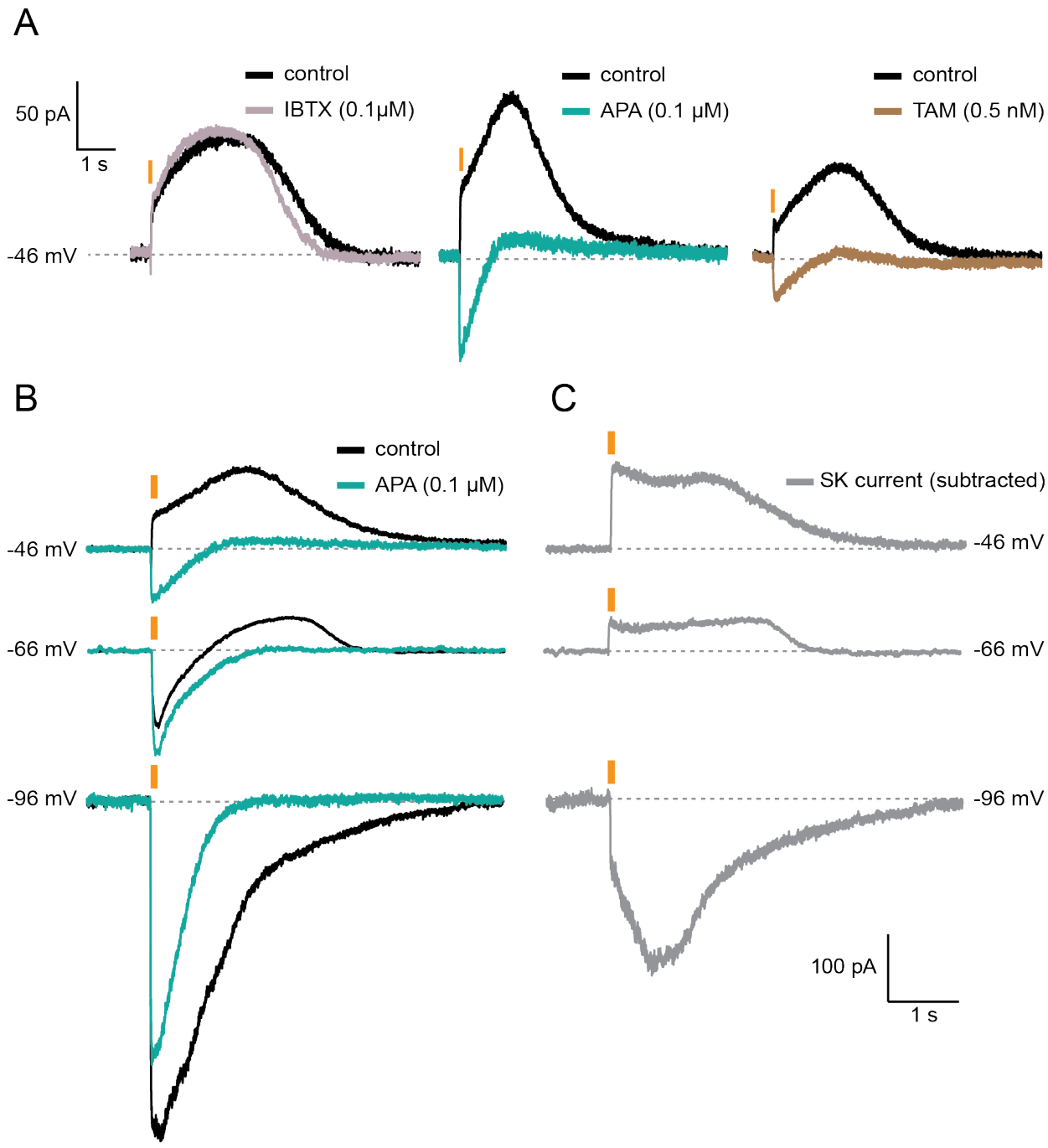

Figure 4 Poppi et al. (2017)

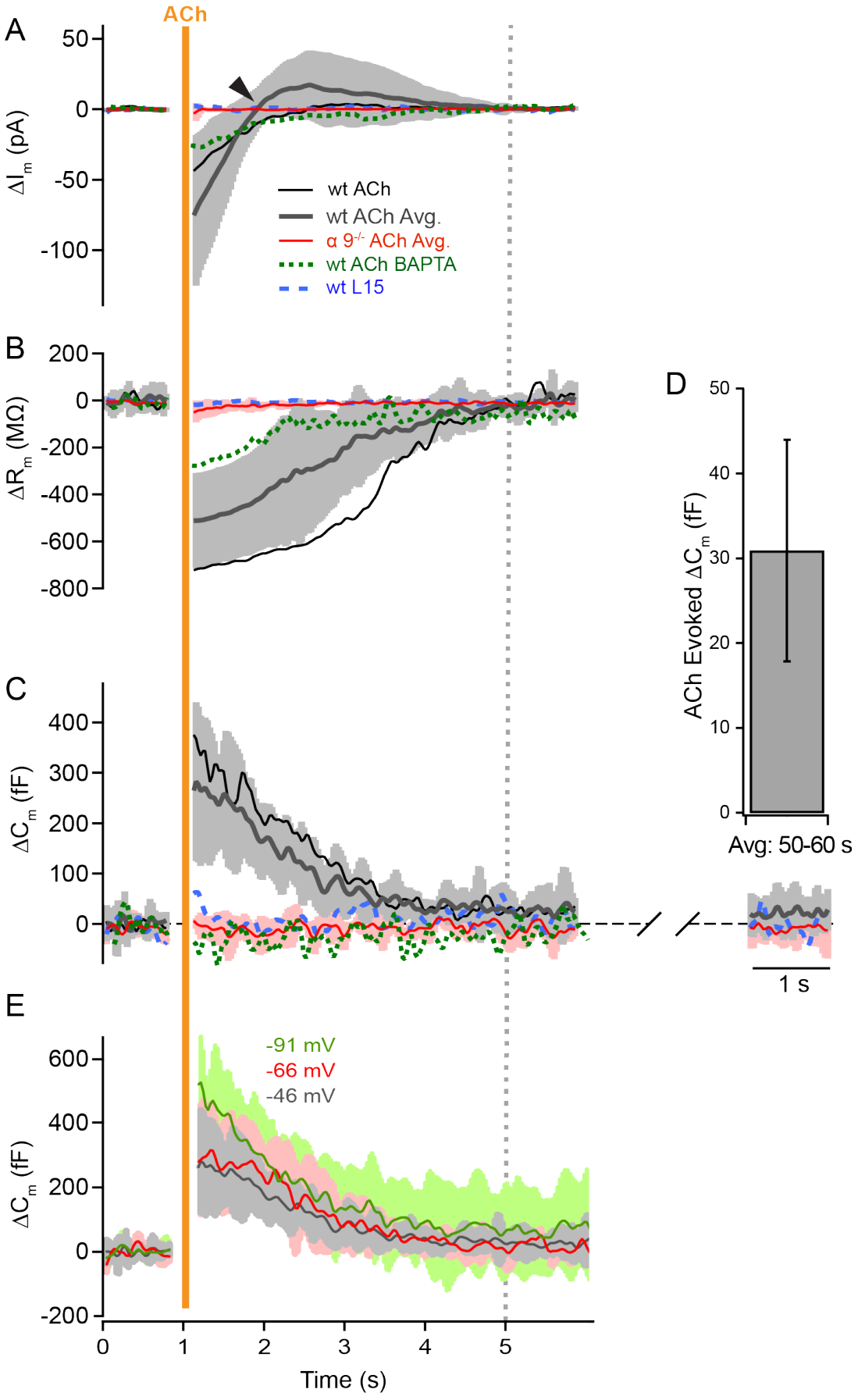

Figure 5 - Poppi et al. (2017) - R2

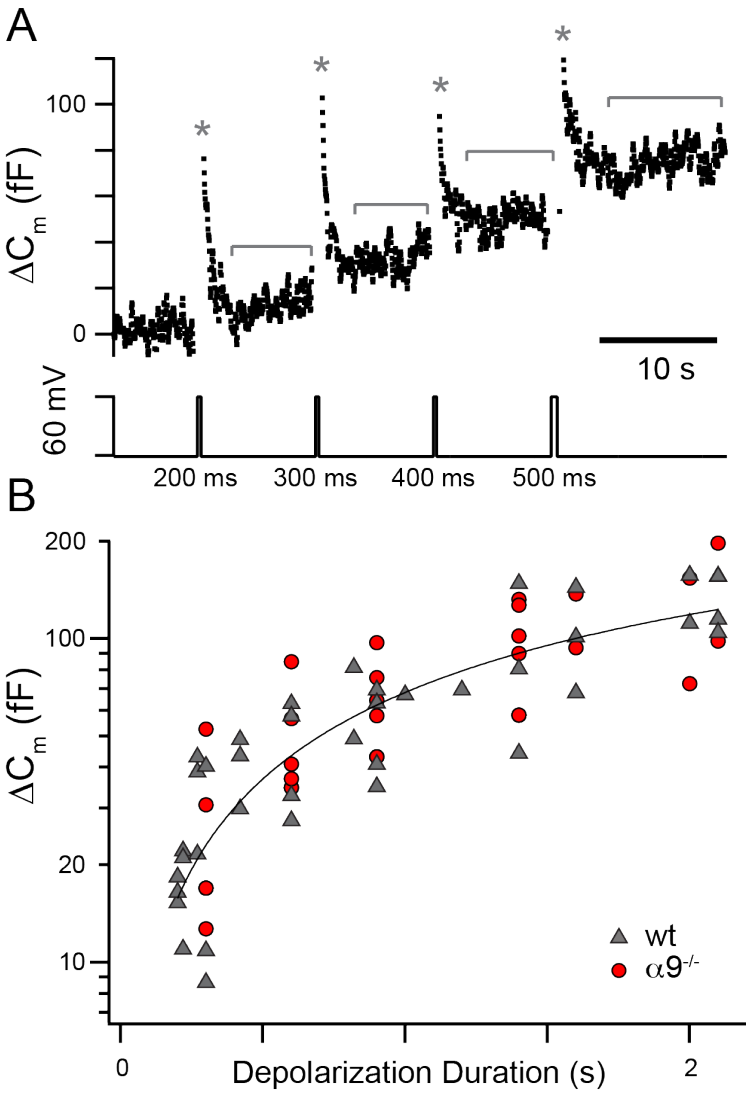

Figure 6 Poppi et al. (2017) - R2

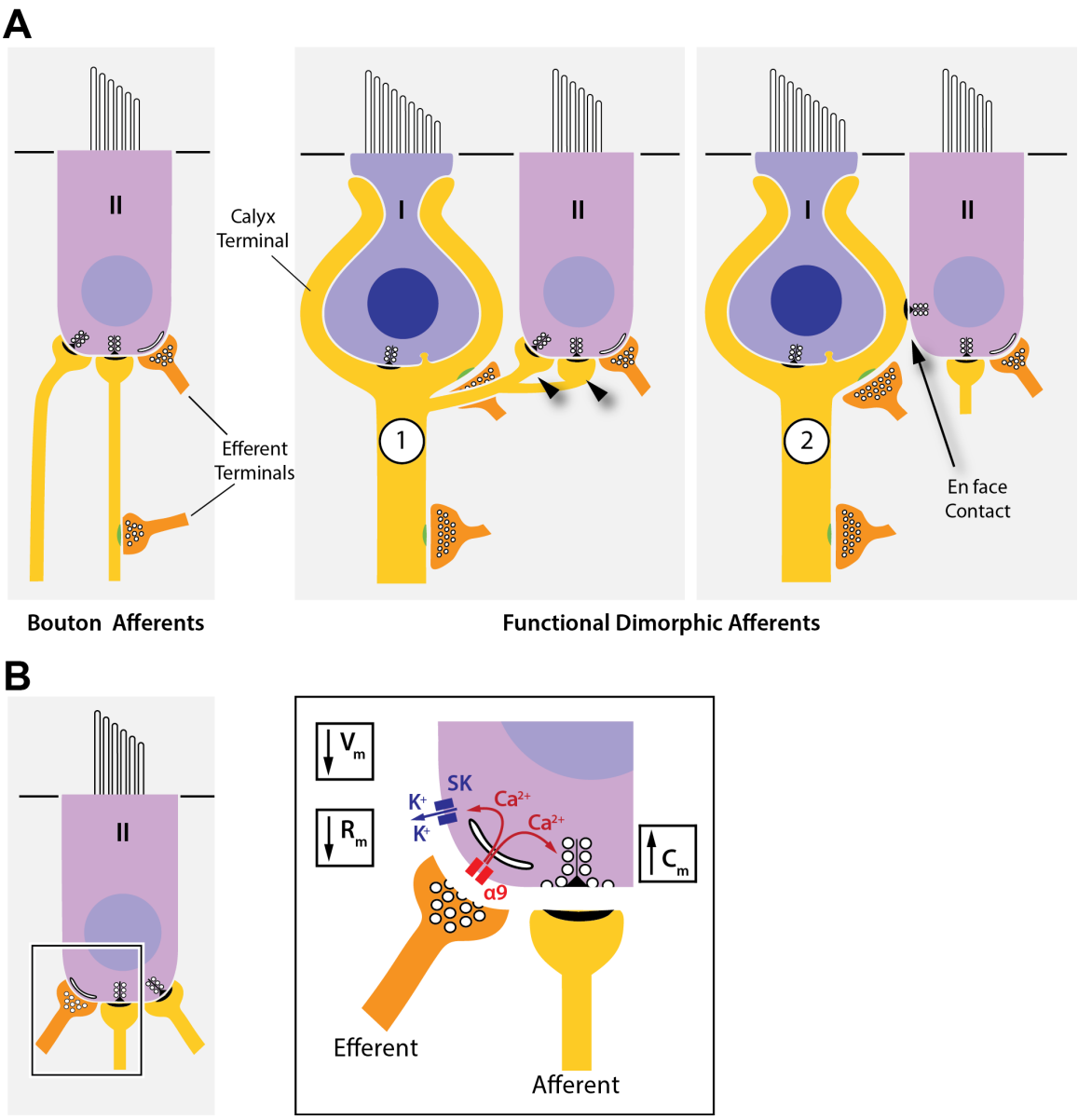

Figure 7 Poppi et al. (2017 – R2)